Polymer 50 (2009) 872–880

Contents lists available at ScienceDirect

Polymer

journal homepage: www.elsevier.com/locate/polymer

Chain confinement in electrospun nanofibers of PET with carbon nanotubes

Huipeng Chen, Zhen Liu, Peggy Cebe*

Department of Physics and Astronomy, Tufts University, 4 Colby Street, Medford, MA 02155, USA

ARTICLE INFO

Article history:
Received 8 August 2008
Received in revised form
12 December 2008
Accepted 15 December 2008
Available online 24 December 2008

Keywords:
Poly(ethylene terephthalate), PET
Electrospun nanofibers
Multiwalled carbon nanotubes

ABSTRACT

Composite nanofibers of poly(ethylene terephthalate), PET, with multiwalled carbon nanotubes (PET/MWCNT) were prepared by the electrospinning method. Confinement, chain conformation, and crystallization of PET electrospun (ES) fibers were analyzed as a function of the weight fraction of MWCNTs. For the first time, we have characterized the rigid amorphous fraction (RAF) in polymer electrospun fibers, with and without MWCNTs. The addition of MWCNTs causes polymer chains in the ES fibers to become more extended, impeding cold crystallization of the fibers, resulting in more confinement of PET chains and an increase in the RAF. The fraction of rigid amorphous chains greatly increased with a small amount of MWCNT loading: with addition of 2% MWCNTs, RAF increased to 0.64, compared to 0.23 in homopolymer PET ES fibers. Spatial constraints also inhibit the folding of polymer chains, resulting in a decrease in crystallinity of PET. For fully amorphous PET/MWCNT composites, MWCNTs do not affect the chain conformation of PET in the ES fibers. For cold crystallized PET/MWCNT composite nanofibers, more trans conformers were formed with the addition of MWCNTs. The increase of RAF (chain confinement) is associated with an increase of the concentration of the trans conformers in the amorphous region as the MWCNT concentration increases in the semicrystalline nanofibers.

1. Introduction

A two-phase model (crystal and amorphous phases) fails adequately to describe the structure of many semicrystalline polymers, including poly(ethylene terephthalate), PET [1–3]. Instead, a three-phase model, comprising crystalline fraction (C), mobile amorphous fraction (MAF), and rigid amorphous fraction (RAF), has been applied in the study of well-crystallized bulk films of PET [1–3], nylon 6 [4], isotactic polystyrene, iPS [5,6], poly(etheretherketone), PEEK [7], poly(phenylene oxide), PPO [8], poly(3-hydroxybutyrate), PHB, poly(carbonate), PC [9,10], and poly(phenylene sulfide), PPS [7]. The RAF contributes neither to the heat of fusion of the crystals nor to the heat capacity change at the glass transition of the mobile amorphous phase. Layers of RAF are considered to be very thin (normally 2–4 nm) compared with those of MAF (normally 10–200 nm) and often suggested to be associated with the lamella crystals as an interfacial layer [1,5]. Because RAF makes its own contribution to the bulk properties of polymers, increasingly, studies have been performed on characterization of RAF [3,6]. However, the effect of nanoparticle fillers on RAF in electrospun fibers, which have very high surface-to-volume ratio, is still unknown. Since RAF has its own distinct properties, it is very useful to realize the effect of nanoparticle fillers on RAF. In this work, we focus on electrospun fibers of PET containing nanoparticle filler.

Especially of interest as a filler material are multiwalled carbon nanotubes (MWCNTs) which have received considerable attention for use as reinforcing elements in polymer based nanocomposites, due to their unique electrical, optical, thermal and mechanical properties along with good thermal and chemical stability. MWCNTs have extremely high elastic modulus which is close to that of diamond [12–14]. Depending on the structure, MWCNTs have a wide range of electrical conductivity. For metallic nanotubes, the electrical current density can be far greater than metals such as silver and copper. The mechanical and electrical properties as well as thermal stability of polymer materials including electrospun (ES) polymer fibers could be highly improved with the incorporation of a very small amount of MWCNTs [15–17].

Since it was patented by Formhals [18–20] in 1934, electrospinning has become an attractive and simple method to produce nanoscale to microscale fibers. It has been used to create drug delivery vehicles, protective clothing, and artificial blood vessels, and in tissue engineering scaffolds, and filtration media. In the electrospinning process, a high voltage is applied to polymer solution or melt. When the electrical force at the surface of a polymer solution or melt overcomes the surface tension, an

* Corresponding author.
E-mail address: peggy.cebe@tufts.edu (P. Cebe).

0032-3861/$ – see front matter © 2008 Elsevier Ltd. All rights reserved.
doi:10.1016/j.polymer.2008.12.030

electrically charged jet of fibers from polymer solution or melt is ejected from the tip of the needle and deposits on the collector [21,22]. These kinds of fibers have several important properties such as high surface-to-volume ratio and good flexibility.

In the present work, we investigate the impact of mutliwalled carbon nanotubes on the properties of PET electrospun fibers. PET is a commercially important engineering thermoplastic with good thermal and mechanical properties. It is used for example in bottles, containers, food packaging, textile fibers, engineering plastics in automobiles, electronics and blood vessel tissue engineering. PET is a typical semicrystalline polymer with a comparatively large amount of RAF. It has been reported that RAF in semicrystalline PET homopolymer films could range from 11% to as high as 44% [1,2]. PET nanocomposite films filled with carbon nanotubes have been studied recently for their potential application in conductive fibers [23], flexible vapor sensors [24] and fuel cells [25,26]. However, the characterization of PET electrospun fibers with CNTs is still unexplored. Here, the chain conformation and crystallization of PET electrospun fibers with the addition of MWCNTs were analyzed. This is the first time that confinement effects, *i.e.*, formation of RAF, have been characterized in polymer electrospun fibers with and without MWCNTs.

2. Experimental section

2.1. Materials

PET films were obtained from the former Allied Signal Corp. with intrinsic viscosity of 0.92 dl/g, measured in 60/40 phenol/trichloroethylene solution, giving a molecular weight of 25,000 g/mol calculated from the Mark-Houwink equation with $a = 0.640$ and $K = 14 \times 10^{-4}$ dl/g. MWCNTs were purchased from MER Corporation. The diameter of the MWCNT is about 140 nm, while the lengths range from 5 μm to 9 μm. The surface of the MWCNT was modified by attaching carboxylic acid functional groups [27–29]. This was done by first suspending the MWCNTs in a mixture of concentrated sulfuric acid and nitric acid (3:1 vol. ratio). Then this solution was sonicated in a Misonix water bath sonicator for several hours at ambient temperature. The resultant suspension was then diluted with 400 mL of deionized water and filtered through a 400 nm pore PTFE membrane until the water passing through the filter had a pH between 6 and 7. The MWCNTs had a purity of 95% after this treatment.

A three-step method was used to disperse the MWCNTs into the polymer solution. Initially the MWCNTs were dispersed in hexafluoro-2-propanol (HFIP) and sonicated 24 h to minimize possible agglomerates. After these treatments, the resulting nanotubes were examined using scanning electron microscopy (SEM). The diameters of MWCNTs remained nearly the same, whereas the lengths of MWCNTs were shortened from 7 ± 2 μm to 5 ± 2 μm. Meanwhile, the PET films were separately dissolved in HFIP and sonicated overnight. Then PET/MWCNT solutions were prepared by mixing these stock solutions to achieve the following weight ratios of MWCNT to PET: 0%, 0.1%, 0.5%, 1% and 2%. PET concentration in homopolymer and 0.1% MWCNT solution is about 20% (w/v) and that of the others is about 10%. The PET/MWCNTs solutions were sonicated overnight before electrospinning.

2.2. Electrospinning process

ES was carried out at room temperature using a 0.5 mm inner diameter glass syringe with a 6 cm working distance. The applied voltages were 15 kV, driven by a high voltage power supply from Gamma High Voltage Research, Inc. model No. ES30P-5W. ES fibers were dried on a heated metal plate at a temperature around 50 °C under a fume hood overnight to effect removal of residual HFIP. The typical bands of HFIP, related to OH stretching vibrations located at 3626 cm^{-1} and 3667 cm^{-1} [30], were not observed in any of the ES fibers.

2.3. Scanning electron microscopy

Morphology of the electrospun fibers was examined using an FESEM Ultra 55 SEM at Harvard University. Samples were fixed to the SEM holder by conducting tape, and were coated with platinum by plasma deposition.

2.4. Thermal analysis

DSC studies were carried out using a TA Instruments temperature modulated DSC (TA Q100). Indium was employed for the temperature and heat flow calibration. The heat capacity was evaluated with respect to sapphire standard. Dry nitrogen gas was purged into the DSC cell with a flow rate of 50 mL/min. DSC measurements were performed at a heating rate of 10 °C/min. Endotherms are presented with downward deflection in our scans.

Three runs were taken to obtain the heat capacity of ES fibers after annealing at 130 °C for 1 h [5,7]. The first run is empty Al sample pan vs. empty Al reference pan to obtain baseline correction. The second run is sapphire standard vs. empty Al reference pan to calibrate heat flow amplitude. The third run is sample vs. the empty reference pan. All the empty Al reference pans and sample pans were kept the same in weight.

To determine the crystallinity of the sample at a given temperature, the sample was heated up to melt at 10 K/min. The crystallinity w_C can be obtained from:

$$w_C = \Delta H(\text{meas})/\Delta H_f \quad (1)$$

where ΔH(meas) is the measured heat fusion of the semicrystalline polymer and $\Delta H_f = 140$ J/g is the heat fusion of 100% crystalline PET [31].

2.5. Wide angle X-ray scattering

WAXS patterns of PET/MWCNT electrospun fiber mats were obtained at room temperature on a Bruker AXS from $2\theta = 8$–$30°$ (for θ the half-scattering angle) at wavelength $\lambda = 0.1545$ nm. Scattered intensity was corrected for air background, and the two-dimensional isotropic pattern was converted to a one-dimensional pattern by integrating over a sector.

2.6. Fourier transform infrared spectroscopy

FTIR absorbance spectra of all ES fibers were collected using a JASCO 6200 spectrometer in attenuated total reflection (ATR) mode. For each measurement, 64 scans were co-added with resolution 4 cm^{-1} in the wavenumber region of 400–4000 cm^{-1}. Curve fitting was performed using the JASCO software.

3. Results and discussion

3.1. Morphology and properties of electrospun fibers

Morphology of the electrospun fibers was examined by SEM, and images are shown in Fig. 1a–e. Only rarely were a few tiny PET beads observed in any of the electrospun fibers. For elimination of PET beads, the solution concentration for homopolymer PET and PET/0.1%MWCNTs required 20% (w/v) of PET to HFIP. Nanocomposites of higher percentages of MWCNTs could be electrospun

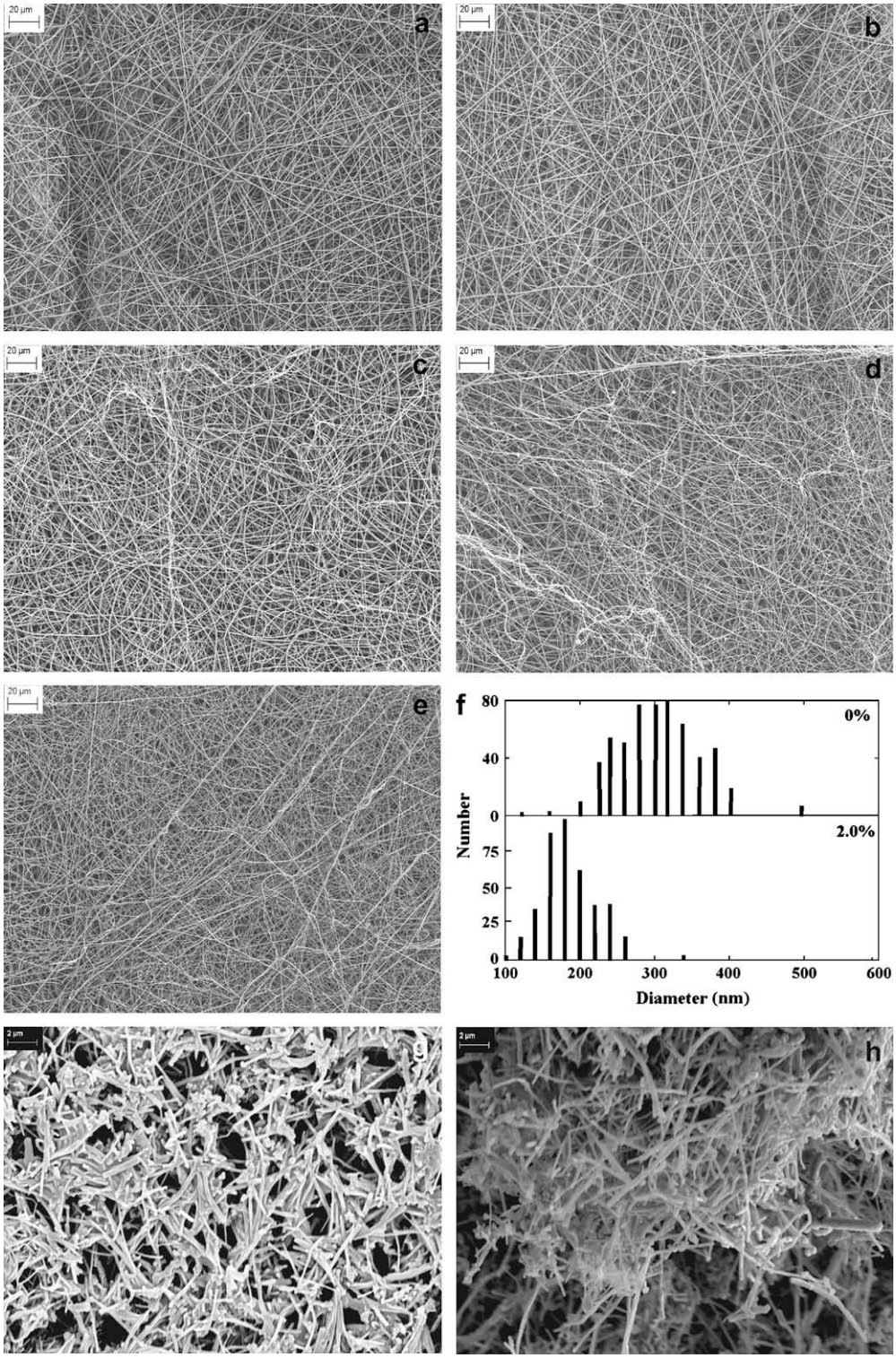

Fig. 1. (a–e) SEM images of untreated, as-spun PET/MWCNT electrospun nanofibers. The weight percent of MWCNTs in the PET/MWCNT composite nanofibers is: (a) 0, (b) 0.1, (c) 0.5, (d) 1.0, and (e) 2.0. (f) Histogram of fiber diameters for ES homopolymer PET nanofibers (top) and 2.0% composite nanofibers (bottom). (g) SEM images of MWCNTs after centrifugation. (h) SEM images of bare MWCNTs.

from solutions of 10% (w/v) of PET to HFIP. The distribution of the diameters of PET ES fibers is displayed in Fig. 1f for 0% (upper frame) and 2% (lower frame) MWCNTs. The diameters of PET homopolymer electrospun fibers ranged from 120 nm to 500 nm, with most fibers around 280–320 nm (see Fig. 1f), compared to the manufacturer's listed average diameter of 140 nm for the MWCNTs. The diameter of electrospun fibers decreased with the addition of MWCNTs from the larger diameter of the homopolymer PET ES fibers. Average diameters of PET ES fibers with 0.5%, 1% and 2% MWCNTs were similar; for 2% the diameters ranged from 100 to 360 nm, and with most fiber diameters around 180 nm (see Fig. 1f).

To demonstrate that the ES fibers contain nanotubes, ES fibers of PET/2%MWCNT were re-dissolved in HFIP and the MWCNTs were recovered by centrifugation. The solution was centrifuged at a rate of 16,000 rev/min for 15 min, and then the HFIP with dissolved PET was decanted, leaving a residue of MWCNTs and some PET. The MWCNT centrifuged deposits were examined by SEM and verified to contain MWCNTs. Results are shown in Fig. 1g. MWCNTs are coated by very thin layers of PET, compared with bare MWCNTs shown in Fig. 1h. Since the length of the nanotubes is much greater than the diameter of the PET ES fibers, they cannot be located transverse to the ES fiber axis. To incorporate the nanotubes into the ES fibers, the nanotube length axis aligns along the PET ES fiber axis, a placement that has been observed previously in other nanocomposite samples using TEM [34–37].

A few ES fibers are too thin to contain a nanotube. These fibers exist in very small number; most fibers have diameters greater than the diameter of the nanotubes themselves. However, since the weight fraction of MWCNTs is small compared to the PET fraction, while their densities are comparable ($\rho_{PET} = 1.37$ g/cm^3 [32]; $\rho_{CNT} = 1.4$ g/cm^3 [33]), the length of the ES fiber is not filled entirely with the nanotubes.

Fig. 2 is an example of a wide angle X-ray diffraction pattern from untreated homopolymer PET ES fibers, also typical of other compositions which are all nearly amorphous after spinning. The WAXS peak from the multiwalled graphene layers could not be seen in the ES fiber patterns, because the concentration of MWCNTs is low. When the purified MWCNTs themselves were examined in WAXS, the graphene layer spacing was observed at $2\theta = 26.2°$ ($d_{002} = 0.34$ nm [38]), indicating that the purification treatments did not alter the multiwall spacing.

Thermal properties of as-spun ES fibers were assessed using standard DSC. Fig. 3 shows the normalized heat flow vs. temperature for different compositions of ES fibers during DSC heating. Equality of the crystallization exotherm and melting endotherm areas also confirms the amorphous nature of the as-spun fibers. Results for crystallization and melting temperatures during heating at 10 °C/min are listed in Table 1. The curves are presented with the same scaling, but are displaced vertically for clarity. The heat flow has been normalized for total sample mass. The crystallization temperature, T_c, decreases from 126 °C for pure PET ES nanofiber to 112 °C for PET/2%MWCNT composite ES nanofiber. In PET/MWCNT composite films MWCNTs act as nucleating agent in crystallization

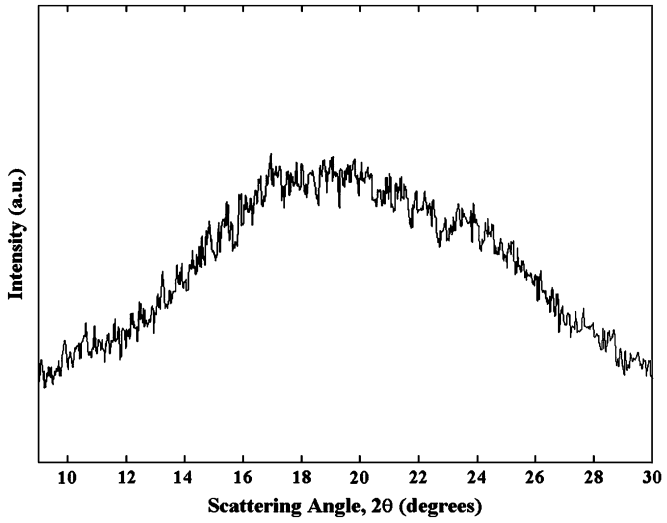

Fig. 2. WAXS intensity vs. scattering angle, 2θ, for untreated, as-spun homopolymer PET electrospun nanofibers. Wavelength $\lambda = 0.154$ nm.

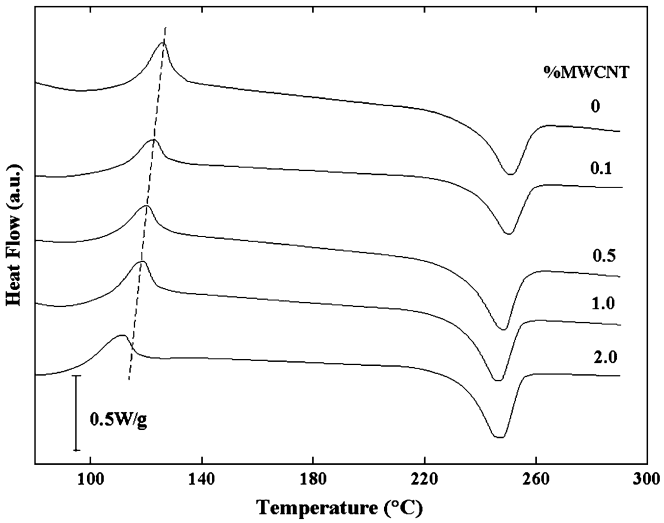

Fig. 3. Heat flow vs. temperature of PET/MWCNT electrospun fibers during DSC heating from 80 °C to the melt at 10 °C/min. The weight percent of MWCNTs in PET/MWCNT composite nanofibers is indicated. Curves are displaced vertically for clarity. The dashed lines are guides to the eye.

[39], resulting in acceleration of the crystallization of PET. Moreover, the melting temperature, T_m, of ES fibers also modestly decreased with an increase of MWCNT concentration. The decrease of T_m results from the decrease of T_c, caused by MWCNT addition.

As shown in Table 1, addition of MWCNTs causes the glass transition temperature of remaining mobile chains to be depressed only slightly suggesting that the mobile amorphous fraction retains the same distribution of relaxation times for the glass to rubbery transition. For polymer/CNT composite films, increase, decrease, or constancy of T_g have all been reported [40–43].

3.2. Characterization of RAF in ES fibers

To crystallize the ES fibers, they were heat treated to 130 °C and cold crystallized for 1 h. Thermal properties of semicrystalline ES fibers, including the glass transition temperature and the crystalline, mobile amorphous, and rigid amorphous fractions, were determined from heat capacity studies (outlined below), and are listed in Table 1. The specific heat capacity of PET/MWCNT electrospun fibers after cold crystallization at 130 °C for 1 h is shown in Fig. 4a–f. We chose this particular temperature to assure that the PET would crystallize quickly and completely. The solid lines represent the values of C_p^{solid} and C_p^{liquid}, taken from the ATHAS data bank [31], which values agree well with the measured data for the heat capacity for homopolymer PET below T_g, and above the melting point, respectively. This close agreement (to within ±2% of homopolymer PET data, which is within the experimental error on the heat capacity measurement) indicates that the heat capacity of PET/MWCNT electrospun fibers is largely unaltered by the small addition of the carbon nanotubes. In Fig. 4, all ES fibers show a tiny lower endotherm, termed an "annealing peak", at about 140 °C, which was formed during cold crystallization at 130 °C.

The PET component is modeled as comprising three portions: a crystal mass fraction, w_C, rigid amorphous fraction, w_{RA}, and a mobile amorphous fraction, w_{MA}. The dashed lines in Fig. 4 represent the calculated heat capacity, C_p^{calc}, for these samples, under the assumption that above T_g all the mobile amorphous fraction, MAF, has relaxed to the mobile liquid state, and only the crystals and RAF remain in the solid state. That is:

Table 1
Thermal properties of PET/MWCNT electrospun nanofibers: crystallization, melting, and glass transition temperatures, and crystal (C), mobile amorphous (MA) and rigid amorphous (RA) fractions.

MWCNT (wt.%)	T_c[a] (°C) ± 0.1	T_m[a] (°C) ± 0.1	T_g[b] (°C) ± 0.1	w_C[b,c] ± 0.01	w_C[b,d] ± 0.01	w_{RA}[b] ± 0.01	w_{MA}[b] ± 0.01
0	126.1	251.3	86.5	0.27	0.27	0.23	0.50
0.1	123.2	250.2	85.8	0.24	0.24	0.26	0.50
0.5	120.2	248.6	85.1	0.14	0.14	0.53	0.32
1.0	118.1	246.8	84.5	0.13	0.13	0.62	0.25
2.0	112.3	247.0	84.3	0.11	0.11	0.64	0.25

[a] Untreated, amorphous ES nanofibers.
[b] ES nanofibers cold crystallized at 130 °C for 1 h.
[c] w_C obtained from Eq. (1).
[d] w_C obtained from Eq. (4).

$$w_S = w_C + w_{RA} = 1 - w_{MA} \quad (2)$$

where w_S is the solid fraction.

The calculation of the heat capacity uses:

$$C_p^{calc}(T) = w_S C_p^{solid}(T) + w_{MA} C_p^{liquid}(T) \quad (3)$$

From Fig. 4 we see that there is good agreement between the calculated heat capacity (dashed line) and the measured data curve just above the glass transition heat capacity step, and furthermore, the slope of the calculated heat capacity lies between the slopes of the (solid) lines for $C_p^{solid}(T)$ and $C_p^{liquid}(T)$. The agreement between C_p^{calc} and experimental C_p allows the solid fraction of all ES fibers at a temperature just above the glass transition to be determined by

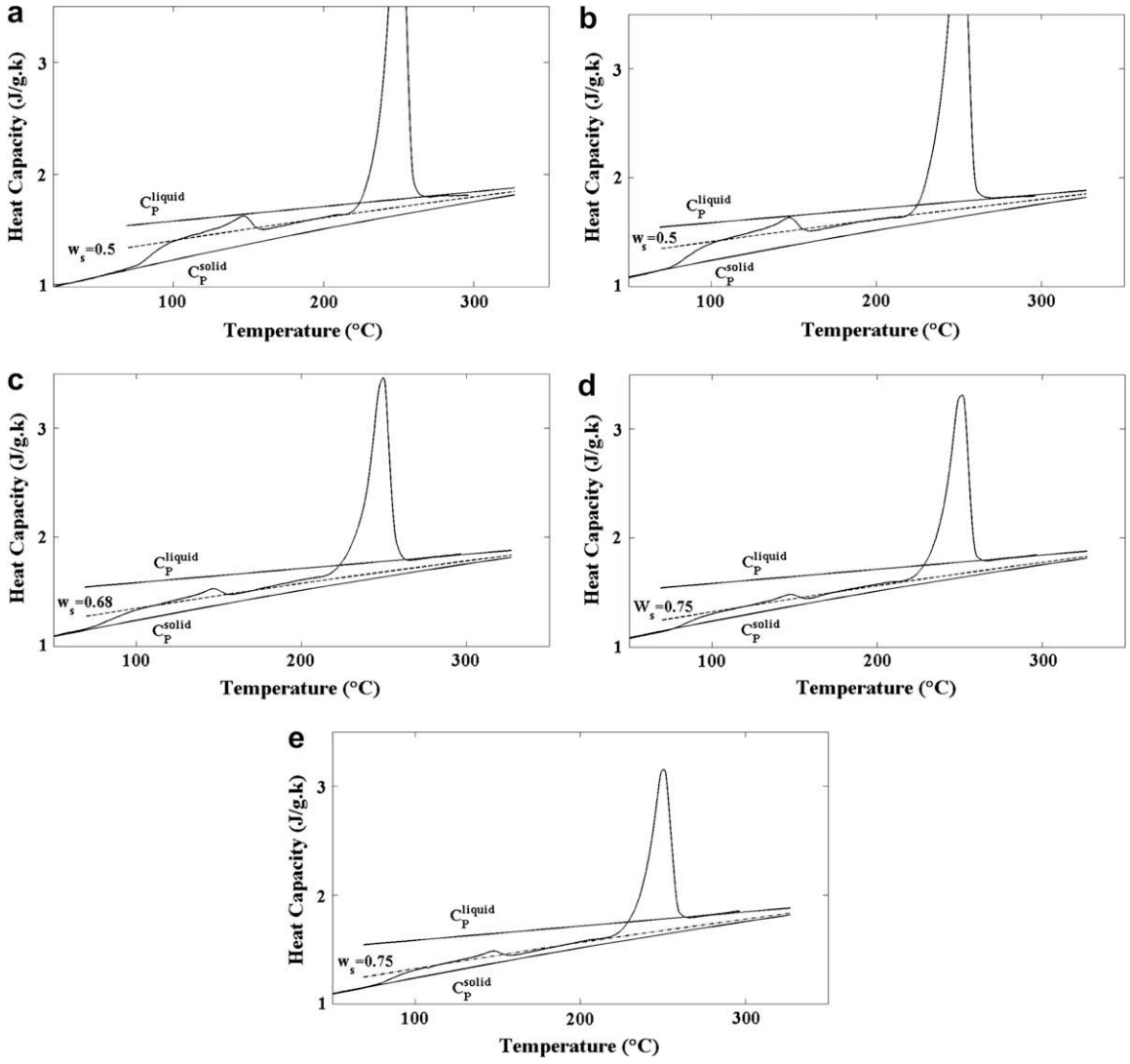

Fig. 4. Specific heat capacity vs. temperature obtained from standard DSC of PET/MWCNT electrospun nanofibers after cold crystallization at 130 °C for 1 h. The weight percent of MWCNTs in PET/MWCNT composite nanofibers is: (a) 0, (b) 0.1, (c) 0.5, (d) 1.0, and (e) 2.0. C_P^{liquid} (solid) is the heat capacity of 100% liquid, while C_P^{solid} (solid) is the heat capacity of 100% solid, using data taken from the ATHAS data bank [30]. Dashed lines are the calculated baseline heat capacity determined from Eq. (3) using the solid fractions, w_S, as indicated.

using Eq. (2) from knowledge of w_{MA}. Since w_S does not change during the traditional glass transition process, w_S remains constant from below the glass transition temperature to just above (50–110 °C). The solid fraction of ES fibers was 0.5 for homopolymer PET, and 0.75 for PET/2%MWCNT from 50 °C to 110 °C, shown in Table 1.

To determine the rigid amorphous fraction using Eq. (2), the crystallinity must also be known. Euler's equation was used to calculate the change of crystallinity with temperature from [44,45]:

$$C_p^{exp}(T) = w_C C_p^{solid}(T) + (1 - w_C) C_p^{liquid}(T) - (dw_C/dT)\Delta H_f(T) \quad (4)$$

where $C_p^{exp}(T)$ is the experimental measured specific heat capacity and $\Delta H_f(T)$ is the temperature dependent heat of fusion corrected for undercooling by the factor $f = 2T/(T + T_m^0)$ [44,45] using 280 °C as the infinite crystal melting point of PET, T_m^0. Crystallinity as a function of temperature results are presented in Fig. 5 for the ES fibers and show that w_C generally decreases through the melting region. The crystallinity at 220 °C is greatest in PET homopolymer ES fibers, and decreases with an increase of MWCNT concentration. The slight increase in w_C above 220 °C seen in samples with 1% and 2% (curves d and e in Fig. 4) occurs as a result of the simplification to a two-phase model, made in the Euler equation [46].

The Euler results for crystallinity at 220 °C match well with the w_C obtained from heat of fusion by Eq. (1), as shown in Table 1. The area of the tiny annealing peak (occurring just below 220 °C) is less than 2% of the area of the main melting peak, and therefore we excluded the annealing peak from the Euler analysis of crystallinity. An error bar was added to the results of w_C to account for the possible tiny contribution of the annealing peak to crystal melting. Assuming w_C remains constant at temperatures below 220 °C, within the error limits, then RAF from low temperature (50 °C, below T_g) to just above glass transition temperature (110 °C) can be determined directly from Eq. (2). Constancy of the crystallinity and the solid fraction from 50 °C to 110 °C result in w_{RA} remaining constant over this temperature interval, and the RAF content at 50 °C is shown in Table 1. w_{RA} increases with an increase of MWCNT concentration. w_{RA} of homopolymer PET ES fibers is close to that seen in cold crystallized PET films [1], which indicates that the fiber morphology in homopolymer PET ES fibers (having diameters of hundreds of nanometers) does not induce any confinement nor does it increase RAF. For PET/2%MWCNT ES fibers, w_{RA} increased to 0.64 which is about three times than that of homopolymer PET ES fibers.

The devitrification of RAF was also assessed from the heat capacity data of Fig. 4. The region from the start of the annealing peak up to the end of the major melting endotherm has usually been examined to determine at what point the RAF relaxes. Along with PET [1,47], other polymers like PPS [11], PPO [8], PHB and PC [9,10] and iPS [48,49] show similar low temperature endotherms after isothermal crystallization or annealing at a temperature between T_g and the melting temperature. For PET film [47], Song stated that the relaxation of RAF occurs between the glass transition and the annealing peak (which Song called the "premelting peak"), *i.e.*, the lowest endotherm seen in the DSC curve. For PPO [8], and iPS studied by rapid scan calorimetry [49], the rigid amorphous fraction was considered to relax (devitrify) only after melting of the crystals. For PHB, PC [9,10], and iPS studied by traditional heating rate DSC [34], the RAF formed at the crystallization temperature and was considered to relax at the lowest endotherm (annealing peak).

In Fig. 4, the calculated heat capacity baseline for w_s of all samples matches well with the measured heat capacity in between the annealing peak and the start of the main crystal melting region. Unchanging solid fraction and unchanging crystallinity mean that the RAF in ES fibers does not devitrify before the start of the main crystal melting. This result is different from that reported in homopolymer PET films, for which RAF totally devitrified at a temperature between the glass transition and the start of main crystal melting [47,50]. The different devitrification kinetics of RAF in the ES fibers, compared to PET bulk films, could be due to the nanoscale fiber morphology which results in differences in molecular chain conformation, as discussed later.

Fig. 6 shows a hypothetical model for the PET/MWCNT electrospun composite nanofiber shown in side view. The dotted line represents the outer diameter of the electrospun fiber and shaded rectangles represent two MWCNTs. In between the two MWCNTs, there are regions of the ES fiber containing only PET chains, represented by the solid lines. The increase of RAF is due to the alignment effect of the MWCNTs: PET chain alignment is enhanced by the co-spinning of MWCNTs with the PET. One possible location for confined chains of PET is at the outer "skin" region, where polymer coats the MWCNTs, whose outer diameter is about 140 nm. The outer diameters of PET/2%MWCNT electrospun fibers range from 120 nm to 240 nm, for a simple average of 180 nm. The close outer diameters will decrease the free volume of polymer chains, resulting in confinement of the polymer chains. The increase in RAF and decrease of w_C might be related to the close diameters of ES fibers and MWCNTs; the narrow space might inhibit the folding of PET chain to form lamellar crystals, which we are presently investigating with small angle X-ray scattering.

Another possibility to explain the increase in RAF is the extension of polymer chains even in the region between the MWCNTs, as depicted in Fig. 6. The impact of MWCNT co-spun with PET may be similar to the impact of rigid-rod molecules. Pan and Liang [51] reported that liquid crystal polymers with rigid-rod segments serve as ordered domains for PET fibers, and these ordered domains increase the degree of orientation of the PET chains. In a similar

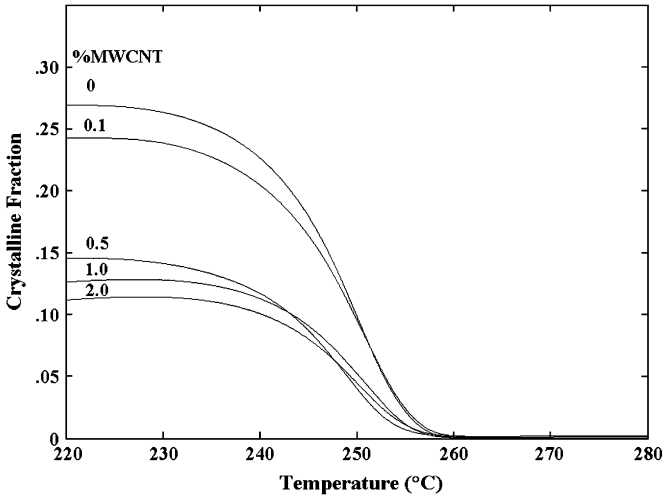

Fig. 5. Crystalline fraction, calculated from Eq. (4), vs. temperature for PET/MWCNT electrospun nanofibers after cold crystallization at 130 °C for 1 h. The weight percent of MWCNTs in PET/MWCNT composite nanofibers is indicated.

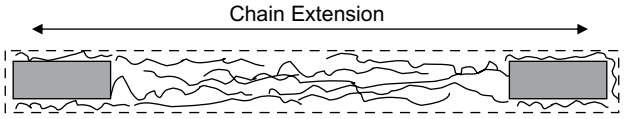

Fig. 6. Schematic representation of the side view of a PET/MWCNT electrospun fiber. Dashed line represents the outer diameter of the electrospun nanofiber and shaded rectangles represent two MWCNTs. Solid lines represent PET polymer chains.

way, rigid-rod-like MWCNTs could serve as oriented domains to enhance the orientation of polymers [52,53]. During the ES process, flexible polymer chains are elongated by the high voltage and will tend to follow the direction of the inflexible oriented domain. Within the ES fiber, the polymer chains might be extended along the axial direction of the MWCNTs embedded in the fiber. The presence of MWCNTs will enhance the extension of each fiber, resulting in a decrease of the mobility of polymer chains, reduction in the degree of crystallinity, and a concomitant increase in RAF.

To investigate the extension of polymer chains, two PET/MWCNTs ES fiber mats were heated to above 200 °C freely floating on oil. The surface area of the ES fiber mat after heating decreased compared to its original surface area, A_0, while the thickness remained constant. Relaxation of the PET chains to a more random-coil conformation occurred after heating. The surface area decreased to $0.48A_0$ for PET ES fiber mat, and decreased to $0.20A_0$ for PET/2%MWCNTs. That means the polymer chains of PET/2%MWCNTs ES fibers were more extended (by more than a factor of two) compared to the chains in PET ES fibers. So the presence of MWCNTs did enhance the extension of polymer chains in ES fibers, resulting in the increase of constrained chains. However, the degree of the chain extension was not high enough to yield strain-induced crystallization, and the crystallinity of the ES fibers decreases with MWCNT addition.

3.3. Chain conformation of ES fibers

Next, we used infrared spectroscopy to examine the conformational isomers present in the PET. There are two kinds of conformational isomers in the PET chain, trans and gauche [39,54–59]. Normally, trans conformers of PET refer to the rotational motions of ethylene diol around the C–C bond. In the crystalline regions of PET, ethylene glycol only shows trans conformers, while in the amorphous region, it mainly shows gauche conformers with a small amount of trans [39]. By using FTIR, Cole and Ajji suggested existence of an intermediate phase in PET linking the crystalline phase to the amorphous phase and mainly constituted of trans conformers [60,61]. Various NMR studies [62–69] on both oriented and unoriented PET have also indicated that there are at least three structures termed the mobile amorphous (characterized mainly by gauche conformers), constrained amorphous or RAF (mainly trans), and crystalline (all trans). Recently, it was reported that for PET/MWCNT nanocomposite films, the presence of MWCNTs induced trans conformers, and the amount of trans conformers in amorphous region decreased with an increase of the MWCNT concentration [39]. They indicated that the addition of carbon nanotubes into PET increased the crystallinity with assistance of trans conformers in amorphous regions, resulting in the overall decrease of trans conformers within amorphous region [39]. We used FTIR spectroscopy to investigate the relative ratio of trans and gauche conformers in PET/MWCNT electrospun fibers.

Fig. 7a and b shows the FTIR results of the untreated, as-spun ES fibers and semicrystalline ES fibers, respectively. The absorption peak at 1174 cm^{-1} has been assigned to the phenyl ring vibration associated with the amorphous region of PET [60,70]. The absorption peak at 1174 cm^{-1} of cold crystallized ES fibers is extremely weak (Fig. 7b) when compared with that of fully amorphous fibers (Fig. 7a). This is related to the decrease of amorphous fraction after cold crystallization.

The absorption peaks at 1340 cm^{-1} and 1370 cm^{-1} are attributed to the CH_2 wagging vibration of the trans ethylene glycol and gauche ethylene glycol, respectively [39]. The relative absorbance ratio of trans conformers at 1340 cm^{-1} to gauche conformers at 1370 cm^{-1}, A_{1340}/A_{1370}, is listed in Table 2.

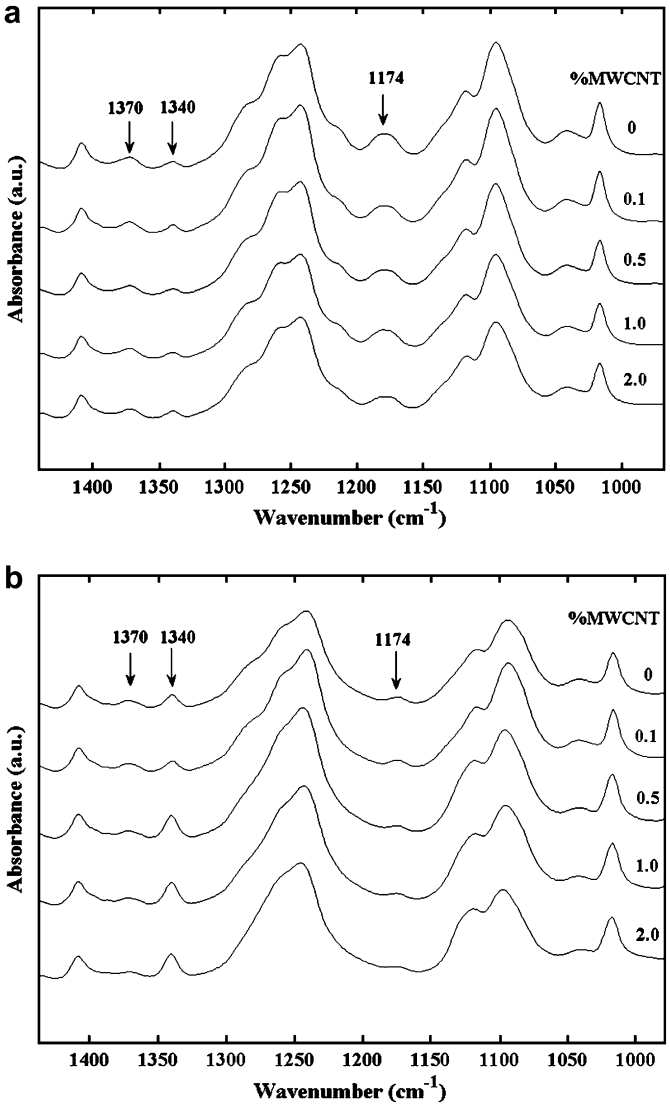

Fig. 7. FTIR absorbance vs. frequency of PET/MWCNT electrospun nanofibers. (a) Untreated, as-spun nanofibers. (b) Nanofibers after cold crystallization at 130 °C for 1 h. The weight percent of MWCNTs in PET/MWCNT composite nanofibers is listed. The CH_2 wagging vibration of trans (1340 cm^{-1}) and gauche (1370 cm^{-1}) conformations, and phenyl ring vibration (1174 cm^{-1}) are indicated.

The equation recently suggested by Zhang and Qian [59,71] to calculate the trans fraction in PET (which included a factor to account for difference in absorptivity of the two vibrations) could not be used in the present work, possibly because of the differences in morphology between their film study and our electrospun fibers. In our work, the trans fraction calculated from the equation of Zhang and Qian was found to be less than the degree of crystallinity. On the assumption that there are only trans conformers within the crystalline region [39,54–59], the fraction of trans conformers

Table 2
Relative infrared absorbance ratio[a] of trans-to-gauche conformations of PET/MWCNT electrospun nanofibers.

MWCNT (wt.%)	0	0.1	0.5	1.0	2.0
A_{1340}/A_{1370}[b]	0.46	0.47	0.45	0.47	0.46
A_{1340}/A_{1370}[c]	1.21	1.32	1.94	2.01	2.35

[a] Trans conformational band at 1340 cm^{-1}; gauche conformational band at 1370 cm^{-1} [29,46].
[b] Absorbance ratio for untreated, amorphous ES nanofibers.
[c] Absorbance ratio for ES fibers cold crystallized at 130 °C for 1 h.

should not be less than the crystalline fraction. Therefore, we elected to use the simple ratio of A_{1340}/A_{1370} to characterize the trans-to-gauche ratio. For untreated, as-spun ES fibers, A_{1340}/A_{1370} is almost constant with MWCNT addition. As mentioned before, the crystallinity of all the untreated, as-spun ES fibers is practically zero from X-ray scattering. This means that for fully amorphous PET/MWCNT electrospun fibers, the MWCNTs do not affect the chain conformation of the amorphous phase of the PET.

However, for semicrystalline ES fibers, A_{1340}/A_{1370} increases with an increase of MWCNT concentration; for example, A_{1340}/A_{1370} of PET/2%MWCNT is two times larger than that of pure PET. The presence of MWCNTs will induce more trans conformers during cold crystallization or annealing, although the presence of MWCNTs does not affect the chain conformation of PET during the electrospinning process (as shown above in Fig. 5).

DSC results show that the crystallinity and mobile amorphous fractions of ES fibers after annealing are smaller, and rigid amorphous fraction is larger, as MWCNT concentration increases. On the other hand, FTIR results show that higher MWCNT concentrations result in formation of more trans conformers. Trans conformers are located in both crystalline and amorphous regions, whereas gauche conformers are only located in amorphous regions. Combining DSC and FTIR results on the cold crystallized ES sample, an increase in MWCNT loading results in an increase of trans conformers, which, because the overall level of crystallinity has *decreased* with MWCNT addition, can only come from an increase of trans conformers within the amorphous fraction. Since the mobile amorphous fraction is also decreased with MWCNT addition, the increase in trans conformers comes from the RAF itself. In electrospun fibers of PET with multiwalled carbon nanotubes, the confinement of the PET chains results in a large increase in RAF, and a concomitant increase in the relative trans-to-gauche conformer ratio.

Regardless of nanotube content, the oriented fiber just after electrospinning is amorphous, and also has no RAF. So, upon heating, the amorphous phase can have complete mobility at T_g and the ratio of trans-to-gauche conformers in the mobile amorphous phase is 0.45–0.47. After cold crystallization, the crystals act as thermoreversible crosslinks to prevent shrinkage: only when the fiber mat is heated to the melt does the area shrinkage occur signaling the PET chain molecular retraction has occurred. Once these crystals are formed, the RAF also forms with the implication that now some of the amorphous fractions cannot express its T_g relaxation. This results in a different distribution of the trans-to-gauche conformers, with ratio now ranging from 1.21 to 2.35, increasing systematically as the RAF fraction increases.

4. Conclusions

Composite nanofibers of poly(ethylene terephthalate), PET, with multiwalled carbon nanotubes were prepared by the electrospinning method using HFIP, which is a good solvent to obtain PET ES nanofibers. Control of solution concentration allows PET composite nanofibers to form with diameters about 1.3 times larger than the diameters of the carbon nanotubes themselves, leading to strong chain confinement effects, and large amount of RAF. Spatial constraints and chain orientation inhibit the folding of polymer chains, resulting in a decrease in crystallinity of PET and an increase of RAF. FTIR was used to examine the chain conformation in PET/MWCNT composite nanofibers. For fully amorphous PET/MWCNT composites, MWCNTs do not affect the chain conformation of PET in the ES fibers. However, once the PET/MWCNT composite nanofibers are cold crystallized, in spite of a reduction of crystallinity, the concentration of trans conformers increased with the addition of MWCNTs. We suggest that the increase of RAF (chain confinement) is associated with the increase in concentration of the trans conformers in the amorphous region, and RAF may be the same as the "intermediate phase" reported previously in PET [62–69].

Acknowledgements

The authors thank the National Science Foundation for support of this work through the Polymers Program of the Division of Materials Research under DMR-0602473 and the MRI Program under DMR-0520655 for thermal analysis instrumentation. The SEM work was carried out at the Harvard University Center for Nanoscale Systems. The authors thank Dr. Georgi Georgiev (Assumption College) for purification of the carbon nanotubes, and Dr. David Wilbur (Tufts University) for the help with preliminary SEM work.

References

[1] Androsch R, Wunderlich B. Polymer 2005;46:12556.
[2] Rastogi R, Vellinga WP, Rastogi S, Schick C, Meijer HEH. J Polym Sci Part B Polym Phys 2004;42:2092.
[3] Arnoult M, Dargent E, Mano JF. Polymer 2007;48:1012.
[4] Chen HP, Cebe P. J Therm Anal Calorim 2007;89:417.
[5] Chen H, Xu H, Cebe P. Polymer 2007;48:6404.
[6] Xu H, Ince BS, Cebe P. J Polym Sci Part B Polym Phys 2003;41:3026.
[7] Huo PP, Cebe P. Macromolecules 1992;25:902.
[8] Pak J, Pyda M, Wunderlich B. Macromolecules 2003;36:495.
[9] Schick C, Wurm A, Mohammed A. Thermochim Acta 2003;396:119.
[10] Schick C, Wurm A, Mohammed A. Colloid Polym Sci 2001;279:800.
[11] Lu X, Cebe P. Polymer 1996;37:4857.
[12] Calvert P. Nature 1999;399:210.
[13] Salvetat JP, Briggs GAD, Bonard JM, Bacsa RR, Kulik AJ, Stockli T, et al. Phys Rev Lett 1999;82:944.
[14] Subramoney S. Adv Mater 1998;10:1157.
[15] Liu TX, Phang IY, Shen L, Chow SY, Zhang WD. Macromolecules 2004;37:7214.
[16] Moniruzzaman M, Winey KI. Macromolecules 2006;39:5194.
[17] McCullen SD, Stevens DR, Roberts WA, Ojha SS, Clarke LI, Gorga RE. Macromolecules 2007;40:997.
[18] Formhals A. US Patent, 1,975,504; 1934.
[19] Formhals A. US Patent, 2,160,962; 1939.
[20] Formhals A. US Patent, 2,187,306; 1940.
[21] Zarkoob S, Eby RK, Reneker DH, Hudson SD, Ertley D, Adams WW. Polymer 2004;45:3973.
[22] Putthanarat S, Eby RK, Kataphinan W, Jones S, Naik R, Reneker DH, et al. Polymer 2006;47:5630.
[23] Li Z, Luo G, Wei F, Huang Y. Comput Sci Technol 2006;66:1022.
[24] Parikh K, Cattanach K, Rao R, Suh DS, Wu A, Manohar SK. Sens Actuators B 2006;113:55.
[25] Wu M, Shaw LL. Int J Hydrogen Energy 2005;30:373.
[26] Wu M, Shaw LL. J Power Sources 2004;136:37.
[27] Jose MV, Steinert BW, Thomas V, Dean DR, Abdalla MA, Price G, et al. Polymer 2007;48:1096.
[28] Xu DH, Wang ZG. Polymer 2008;49:330.
[29] Zeng HL, Cao C, Wang YP, Watts PCP, Kong H, Cui XW, et al. Polymer 2006;47:113.
[30] Schaal H, Haber T, Suhm MA. J Phys Chem 2000;104:265.
[31] Pyda M, editor. ATHAS data bank, http://athas.prz.edu.pl; 1997.
[32] Braundrup J, Immergun E. Polymer handbook. New York: John Willey & Sons; 1980.
[33] Collins PG, Avouris P. Sci Am 2000;283:62.
[34] Zhou WP, Wu YL, Wei F, Lou GH, Qian WZ. Polymer 2005;46:12689.
[35] Zhang QH, Chang ZJ, Zhu MF, Mo XM, Chen DJ. Nanotechnology 2007;18:115611.
[36] Ayutsede J, Gandhi M, Sukigara S, Ye HH, Hsu CM, Gogotsi Y, et al. Biomacromolecules 2006;7:208.
[37] Dror Y, Salalha W, Khalfin RL, Cohen Y, Yarin AL, Zussman E. Langmuir 2003;19:7012.
[38] Saito Y, Yoshikawa T, Bandow S, Tomita M, Hayashi T. Phys Rev B 1993;48:1907.
[39] Tzavalas S, Drakonakis V, Mouzakis DE. Macromolecules 2006;39:9150.
[40] Meng H, Sui GX, Fang PF, Yang R. Polymer 2008;49:610.
[41] Gregoriou VG, Kandilioti G, Bollas ST. Polymer 2005;46:11340.
[42] Zhao CG, Hu GJ, Justice R, Schaefer DW, Zhang SM, Yang MS, et al. Polymer 2005;46:5125.
[43] Kuila BK, Malik S, Batabyal SK, Nandi AK. Macromolecules 2007;40:278.
[44] Pyda M, Di Lorenzo M, Park J, Kamasa P, Buzin A, Grebowicz J, et al. J Polym Sci Part B Polym Phys 2001;39:1565.
[45] Di Lorenzo M, Pyda M, Wunderlich B. J Polym Sci Part B Polym Phys 2001;39:1594.

[46] Mathot VBF. Calorimetry and thermal analysis of polymers. Cincinnati: Hanser Gardner Publications, Inc.; 1994.
[47] Song M. J Appl Polym Sci 2001;81:2779.
[48] Xu H, Cebe P. Macromolecules 2004;37:2797.
[49] Minakov A, Mordvintsev D, Tol R, Schick C. Thermochim Acta 2006;442:25.
[50] Chen HP, Cebe P. Macromolecules 2008. doi:10.1021/ma802104a.
[51] Pan LH, Liang B. J Appl Polym Sci 1998;70:1035.
[52] Prilutsky S, Zussman E, Cohen Y. Nanotechnology 2008;19:165603.
[53] Salalha W, Dror Y, Khalfin RL, Cohen Y, Yarin AL, Zussman E. Langmuir 2004;20:9852.
[54] Miyake A. J Polym Sci 1959;38:479.
[55] Manley TR, Williams DA. Polymer 1969;10:339.
[56] Ward IM, Wilding MA. Polymer 1977;18:327.
[57] Daubeny R, Bunn CW, Brown CJ. Proc R Soc London 1954;226:531.
[58] Lu XF, Hay JN. Polymer 2001;42:8055.
[59] Zhang Y, Zhang JM, Lu YL, Duan YX, Yan SK, Shen DY. Macromolecules 2004;37:2532.
[60] Cold KC, Ajji A, Pellerin E. Macromolecules 2002;35:770.
[61] Ajji A, Guevremont J, Cole KC, Dumoulin MM. Polymer 1996;37:3707.
[62] Havens JR, VanderHart DL. Macromolecules 1985;18:1663.
[63] Tzou DL, Desai P, Abhiraman AS, Huang TH. J Polym Sci Part B Polym Phys 1991;29:49.
[64] Tzou DL, Desai P, Abhiraman AS, Huang TH. J Polym Sci Part B Polym Phys 1995;33:63.
[65] Wilhelm M, Spiess HW. Macromolecules 1996;29:1088.
[66] Kawaguchi T, Mamada A, Hosokawa Y, Horii F. Polymer 1998;39:2725.
[67] Miwa Y, Takahashi Y, Kitano Y, Ishida H. J Mol Struct 1998;441:295.
[68] Huang JM, Chu PP, Chang FC. Polymer 2000;41:1741.
[69] Bai S, Hu JZ, Pugmire RJ, Grant DM, Taylor CMV, Rubin JB, et al. Macromolecules 1998;31:9238.
[70] Stokr J, Schneider B, Doskocilova D, Lovy J, Sedlacek P. Polymer 1982;23:714.
[71] Qian RY, Shen DU, Sun FG, Wu LH. Macromol Chem Phys 1996;197:1485.